Int. J. Electrochem. Sci., 7 **(2012)** 6453 - 6464

International Journal of
ELECTROCHEMICAL
SCIENCE
www.electrochemsci.org

High Rate Performance of $LiM_{0.1}Mn_{1.9}O_4$ (M=Mn, Al, Fe) as Cathodes of Lithium Ion Battery at 25°C and 55°C

Bin Cheng, Xianglan Chen, Xiaowei Li, Huayun Xu[*], *Jian Yang, Yitai Qian*

Key Laboratory of the Colloid and Interface Chemistry (Shandong University), Ministry of Education, and School of Chemistry and Chemical Engineering, Shandong University, Jinan 250100, PR China
[*]E-mail: xuhuayun@sdu.edu.cn

Received: 6 March 2012 / *Accepted:* 2 June 2012 / *Published:* 1 July 2012

$LiM_{0.1}Mn_{1.9}O_4$ (M=Mn, Al, Fe) compounds were synthesized via a sol–gel process. The XRD pattern indicates that the samples could be indexed as a spinel structure without any impurities. The doped Al and Fe can be clearly observed on the surface of the samples from the energy dispersive spectrometer (EDS) images. The TEM images show that the particle size is about ~ 100nm. The SEM images reveal the particles aggregated into porous structures. Textural analysis was carried out by measuring the N_2 adsorption/desorption isotherms. Among the samples, the galvanostatic charge–discharge testing shows that $LiAl_{0.1}Mn_{1.9}O_4$ sample exhibits the best electrochemical performance at high rate and at high temperature. A typical $Li/LiAl_{0.1}Mn_{1.9}O_4$ cell shows a discharge capacity of 95.8mAh g^{-1} at 50C discharge rate (charged at 5C) at 25°C. Even at 55°C, 85.0% of the discharge capacity is maintained at a rate of 5C after 200 cycles. In addition, the influences of doping Al and Fe on the electrochemical performance of $LiMn_2O_4$ are characterized by cyclic voltammetry (CV) and electrochemical impedance spectroscopy (EIS).

Keywords: Doped $LiMn_2O_4$; Sol–gel method; Rate capability; Lithium ion battery

1. INTRODUCTION

How to improve the high energy and power density capability of lithium ion battery is attracting widespread research over the past few years due to potential applications in both electric vehicles (EVs) and hybrid electric vehicles (HEVs) [1,2].

The improvement of the specific power density in lithium battery is a fundamental issue to solve the above problem. $LiMn_2O_4$ is a promising cathode of lithium ion battery to replace layered Ni or Co oxide materials because of its significant advantages, such as excellent rate capability, environmental friendliness and low cost [3].

The nanostructured morphologies of $LiMn_2O_4$ could meet the requirements for application in high power systems [4,5]. However, plain $LiMn_2O_4$ shows poor cycling stability, especially quick fading of capacity at a higher temperature above 55°C [6].

Various methods have been developed to increase the electrochemical performance of $LiMn_2O_4$, such as coating [7,8] and doping [9-22]. And it has well been demonstrated that the electrochemical properties of $LiMn_2O_4$ could be improved by partial substitution of Mn^{3+} with several elements, such as Co [10,11], Cr [12], Zn [13], Ce [14], Li [15] Al [16-20], Fe [21,22] etc. Lee et al reported that Al–doped spinel ($LiAl_xMn_{2-x}O_4$) obtained 128 mAh g^{-1} for the first cycle and 115 mAh g^{-1} after 100 cycles with a discharge current of 0.4 mA cm^{-2} [16]. Hwang et al investigated the effect of Al–doped on the stability of $LiMn_2O_4$ spinel. The initial discharge capacity and 10th discharge capacity were about of 100 mAh g^{-1} and 90 mAh g^{-1} at 0.1C charge–discharge rate [17]. Bang et al. reported that Fe improve the capacity retention ratios from 70% to 96% after 30 cycles [21]. It is clear that doping Al and Fe can play a role in stabling the structure to improving the capacity retention. However, fast charge and discharge performance especially at elevated temperature was lack for most published Al or Fe doping $LiMn_2O_4$ literatures.

In our study, $LiM_{0.1}Mn_{1.9}O_4$ (M=Mn, Al, Fe) materials were synthesized by a sol–gel method. The XRD pattern indicates the samples are in a spinel structure. The grains around ~ 100nm aggregate into porous structures showed by SEM. The N_2 adsorption/desorption experiments show the similar big surface area compared to the porous nanorods reported previously [23]. Among the three samples, $LiAl_{0.1}Mn_{1.9}O_4$ exhibits the best electrochemical performances showing a discharge capacity of 95.8mAh g^{-1} at 50C discharge rate (charged at 5C) at 25°C. Even at 55°C, capacity retention of 85.0% after 200 cycles at 5C charge–discharge rate is obtained for this electrode. The diffusion coefficient of Li^+ (D_{Li}) calculated from cyclic voltammograms (CVs) is in the range of 10^{-8}–10^{-7} cm^2 s^{-1}. The Faradic charge–transfer resistance (R_{ct}) and the Warburg impendence (Z_w) are investigated by fitting the impedance data with ZSimpWin software. The good electrochemical performance of $LiAl_{0.1}Mn_{1.9}O_4$ is in agreement with data of CV and EIS.

2. EXPERIMENTAL

2.1. Preparation of materials

The $LiM_{0.1}Mn_{1.9}O_4$ (M=Mn, Al, Fe) were prepared by the sol–gel method using citric acid and glycol as the chelating agent.

The stoichiometric amount of $LiNO_3$ (CP), 50% $Mn(NO_3)_2$ solution (AR), $Al(NO_3)_3 \cdot 9H_2O$ (AR), $Fe(NO_3)_3 \cdot 9H_2O$ (AR) were mixed with citric acid (AR) and glycol (AR) which their molar ratio was kept as 1:4 dissolved in 20mL of distilled water. The molar ratio of metal ion to citric acid was 1:1. Then the solution was stirred at 80°C for 2h, and the obtained gel was dried in air oven at 180°C for 10h. After that, it was sintered at 700°C for 10h in air at a heating rate of 5°C min^{-1} then cooled to room temperature naturally in the oven.

2.2. Characterization of $LiM_{0.1}Mn_{1.9}O_4$ (M=Mn, Al, Fe) compounds

X-ray diffraction was carried out by an advanced X-ray diffractometer of Bruker D8 based on Ni-filtered Cu Kα-radiation (λ=1.5418 Å). The particle morphologies were examined using a transmission electron microscope (TEM, JEM–1011) and a field emission scanning electron microscope (FESEM, JEOL JSM–6700F). The EDS used the same FESEM (JEOL JSM–6700F) instrument. The N_2 adsorption/desorption experiment was carried out by using a QuadraSorb SI surface area analyzer at 77 K. Cyclic voltammetry experiments were carried out between 3.4~4.3 V at a scan rate of 0.1 mV s^{-1} using a LK2005A Electrochemical Workstation. EIS were performed by a Zahner Elektrik IM6 (Germany) impedance instrument over the frequency range of 100 kHz to 0.01 Hz.

2.3. Preparation and electrochemical testing of composite electrodes

The composite electrodes were prepared as follow: active material, acetylene black and PVDF binder in the ratio of 80: 10: 10 respectively with N–methyl–2–pyrollidone were mixed completely to form slurry.

The slurry was coated onto an Al-foil current collector, and dried at 80°C for 12h and finally roll pressed to ca. 0.6 mm thick. The coin cells of type CR2032 were made in Ar-filled glove box using lithium metal foil as the counter and the reference electrode. The electrolyte used was $LiPF_6$ in ethylene carbonate (EC), diethyl carbonate (DEC), dimethyl carbonate (DMC) in the ratio of 1:1:1 by volume.

The galvanostatic studies were carried out with a LAND CT2001A auto–cycler (China) in the voltage range of 3.4~4.3V at 25°C and at 55°C. The cells were cycled at current rate 1C and 5C (1C≈148mA g^{-1}).

3. RESULTS AND DISCUSSION

3.1 Structure characterization and morphology observation

3.1.1. Structure characterization

Fig.1 shows the XRD patterns of $LiM_{0.1}Mn_{1.9}O_4$ (M=Mn, Al, Fe) compounds. All the peaks in these XRD patterns could be assigned to a spinel structure. No impurities such as Al_2O_3 and Fe_2O_3 are detected. The calculated lattice constant of $LiMn_2O_4$, $LiAl_{0.1}Mn_{1.9}O_4$ and $LiFe_{0.1}Mn_{1.9}O_4$ are 8.234(2) Å, 8.210(7) Å and 8.232(5) Å, respectively. This lattice contraction indicates the successful substitution of Al and Fe for Mn in the products. EDS images for element analyses were shown in Fig. 2. The doped Al and Fe can be clearly observed on the surface of the samples in Fig. 2b and Fig. 2c, respectively.

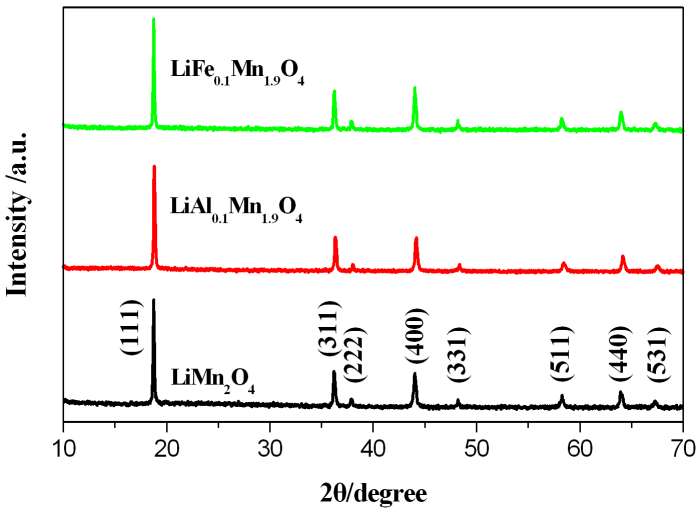

Figure 1. X–ray diffraction patterns of $LiMn_2O_4$, $LiAl_{0.1}Mn_{1.9}O_4$ and $LiFe_{0.1}Mn_{1.9}O_4$

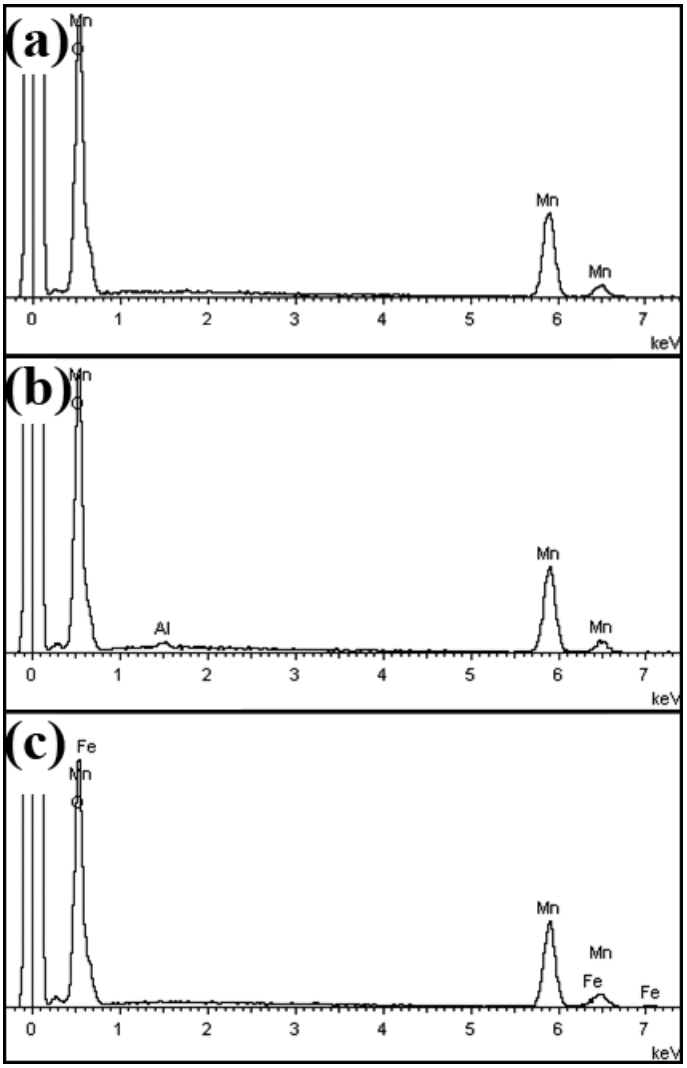

Figure 2. EDS of (a) $LiMn_2O_4$, (b) $LiAl_{0.1}Mn_{1.9}O_4$ and (c) $LiFe_{0.1}Mn_{1.9}O_4$

3.1.2. Morphology observation

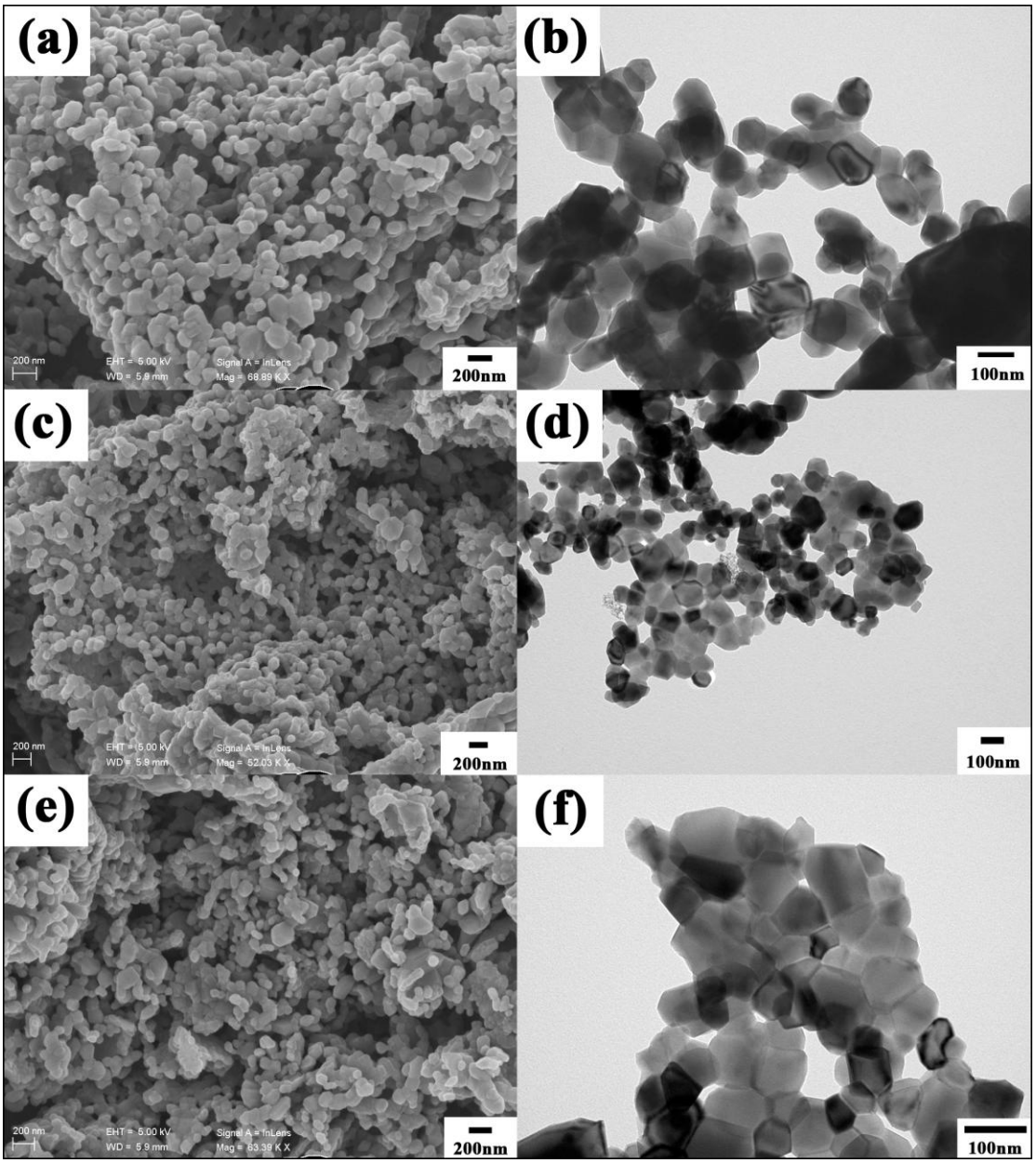

Figure 3. SEM micrographs of the as–prepared (a) $LiMn_2O_4$, (c) $LiAl_{0.1}Mn_{1.9}O_4$, (e) $LiFe_{0.1}Mn_{1.9}O_4$. TEM images of the samples (b) $LiMn_2O_4$, (d) $LiAl_{0.1}Mn_{1.9}O_4$, (f) $LiFe_{0.1}Mn_{1.9}O_4$

The surface morphology and particle size were investigated by TEM and SEM. From Fig. 3a-3f, TEM shows a uniform particle size around 100 nm for the prepared materials and porous structures formed by aggregation of particles are observed through SEM. Textural analysis was carried out by the N_2 adsorption/desorption experiments. The testing results of samples are summarized in Table 1. The surface area are similar to the results of porous $LiMn_2O_4$ nanorods (8.6 $m^2 g^{-1}$) previously reported by Cheng et al [23] and larger than the values of Co doped $LiMn_2O_4$ (2.1 $m^2 g^{-1}$) reported by Sakunthala et al [3]. The uniform particle size and relatively big surface area are advantageous to improving the discharge capacity and rate capability for $LiMn_2O_4$ material.

Table 1. The parameters from N_2 adsorption/desorption experiment for the samples.

Sample	Surface Area (m^2 g^{-1})	Pore Volume (cc g^{-1})	Pore Diameter Dv(d) (nm)
$LiMn_2O_4$	9.317	0.011	3.285
$LiAl_{0.1}Mn_{1.9}O_4$	6.976	0.009	4.123
$LiFe_{0.1}Mn_{1.9}O_4$	7.874	0.008	3.214

3.2 Galvanostatic cycling studies

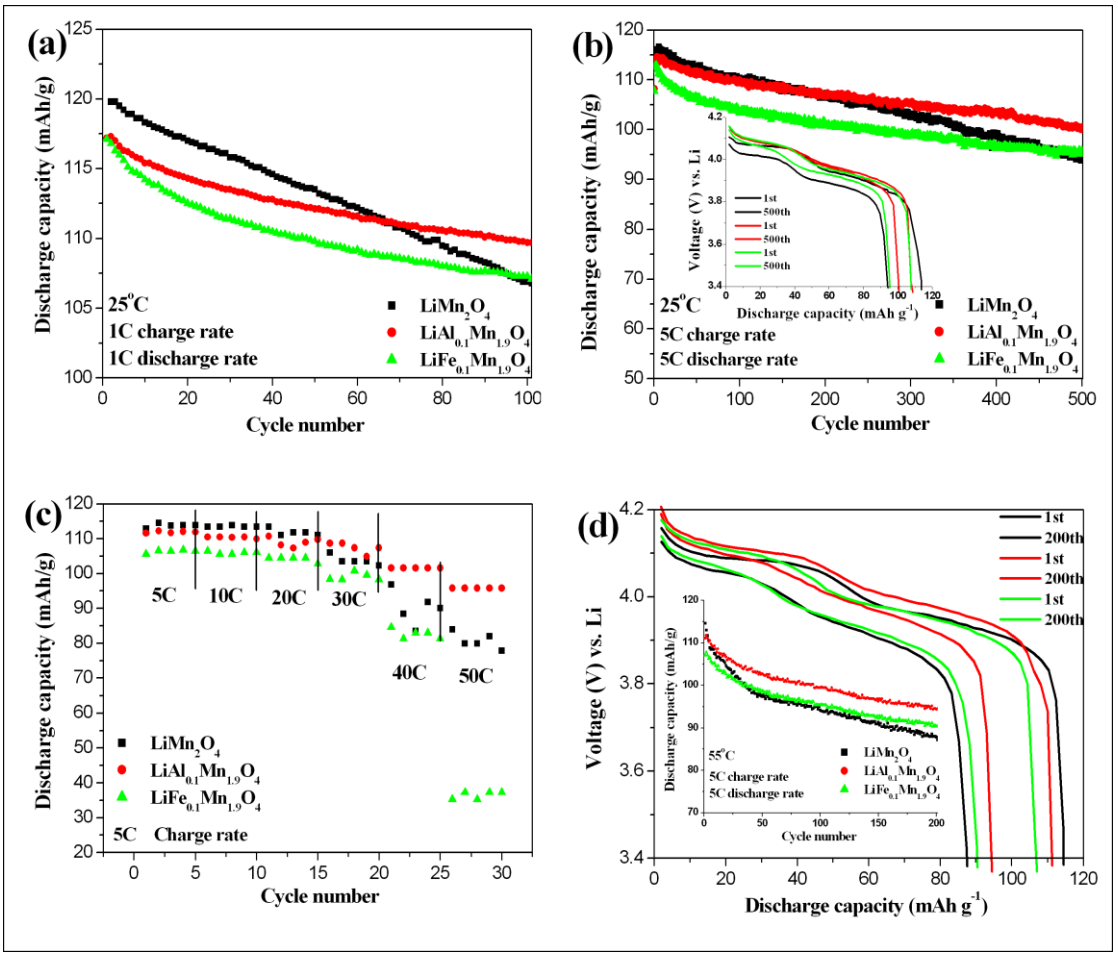

Figure 4. (a) The cycle performance of electrodes in the voltage range of 3.4~4.3 V at 1 C rate; (b) Discharge capacity vs. cycle number of samples at 5C rate at 25℃, inset is the discharge plateaus of 1st and 500th; (c) Rate performance of the discharge capacity of electrodes at varied discharge rate from 5 to 50C and at charged at 5C**;** (d) The discharge plateaus of 1st and 200th for the samples charge–discharge at 5C rate at 55℃, inset is the cycle performance of electrodes

Fig. 4a and Fig. 4b represent the cycling performances of $LiMn_2O_4$, $LiAl_{0.1}Mn_{1.9}O_4$ and $LiFe_{0.1}Mn_{1.9}O_4$ cathode materials between 3.4 and 4.3V at 1C and 5C rate at 25°C, respectively. The pristine $LiMn_2O_4$ shows slightly larger discharge capacities than those of doped samples and then deteriorates in the following tests. Compared with $LiFe_{0.1}Mn_{1.9}O_4$ sample, the $LiAl_{0.1}Mn_{1.9}O_4$ exhibits

better cycle performance. Seen form inset of Fig. 4b, the discharge plateaus of doped $LiMn_2O_4$ samples shift toward higher potential than those of pure $LiMn_2O_4$. To further investigate the application for high power density devices, the electrodes were discharged at rates ranging from 5C to 50C with 5C charge rate.

Table 2. The electrochemical performance of the $LiMn_2O_4$, $LiAl_{0.1}Mn_{1.9}O_4$ and $LiFe_{0.1}Mn_{1.9}O_4$

Sample	25°C				55°C	
	1C		5C		5C	
	*	**	*	***	*	****
$LiMn_2O_4$	119.8	106.8/89.1	112.0	93.0/83.0	114.6	87.2/76.1
$LiAl_{0.1}Mn_{1.9}O_4$	117.3	109.7/93.5	108.2	100.6/92.4	111.1	94.6/85.0
$LiFe_{0.1}Mn_{1.9}O_4$	116.8	107.1/91.7	107.7	95.3/88.5	107.1	90.6/84.5

Note:
* Initial discharge capacity (mAh g^{-1});
** 100th cycle discharge capacity (mAh g^{-1})/retention of discharge capacity (%);
*** 500th cycle discharge capacity (mAh g^{-1})/retention of discharge capacity (%);
**** 200th cycle discharge capacity (mAh g^{-1})/retention of discharge capacity (%).

Among the three samples, $LiAl_{0.1}Mn_{1.9}O_4$ exhibits the best electrochemical performance at high rate. As shown in Fig. 4c, the Li/$LiAl_{0.1}Mn_{1.9}O_4$ cell exhibits relatively high specific capacity at 50C discharge rate (5C: 111.6 mAh g^{-1}, 10C: 110.5 mAh g^{-1}, 20C: 110.7mAh g^{-1}, 30C: 109.8 mAh g^{-1}, 40C: 101.6 mAh g^{-1}, 50C: 95.8 mAh g^{-1}, respectively). Fig. 4d shows the typical galvanostatic discharge profiles and the cycling performance (inset of Fig. 4d) of three spinel materials tested at 5C charge–discharge rate at 55°C. The $LiAl_{0.1}Mn_{1.9}O_4$ also represents the best electrochemical performance at high temperature. The good electrochemical property is due to the stronger bond energy of Al–O (~501.9 kJ mol^{-1}) than Mn–O (~362 kJ mol^{-1}) [24] and Fe–O (~409 kJ mol^{-1}) [25], which stabilized the structure during cycling. The electrochemical performance of the samples is summarized in Table 2.

3.3 Cyclic voltammetry studies

We have performed a series of voltammetry measurements of the prepared spinel electrodes in order to gain further insight into the electrochemical characteristics. Fig. 5a–5c show the CVs of the $LiMn_2O_4$, $LiAl_{0.1}Mn_{1.9}O_4$ and $LiFe_{0.1}Mn_{1.9}O_4$ recorded at different potential sweeping rates 0.1, 0.2, 0.3, 0.5, 0.7 and 1 mV s^{-1}. All electrodes show increasing peaks current density (I_p) and widening separation potential within each redox couple as the potential scanning rate (v) increases. Assuming that the intercalation reaction is controlled by the solid-state diffusion of lithium ions, the dependence of I_p on $v^{1/2}$ can be applied to determine the D_{Li} on the basis of the following equation [23]: $I_p=2.69\times10^5 n^{3/2} D_{Li}^{1/2} v^{1/2} C^0_{Li}$ .Where n is the number of electrons per reaction species and C^0_{Li} is the bulk concentration of Li^+ in the electrode (given as 0.02378mol cm^{-3} from the theoretical density of

spinel). Good linear relationship between I_p and $v^{1/2}$ is observed for the investigated samples (Fig. 6a) and the calculated D_{Li} values are summarized in Table 3.

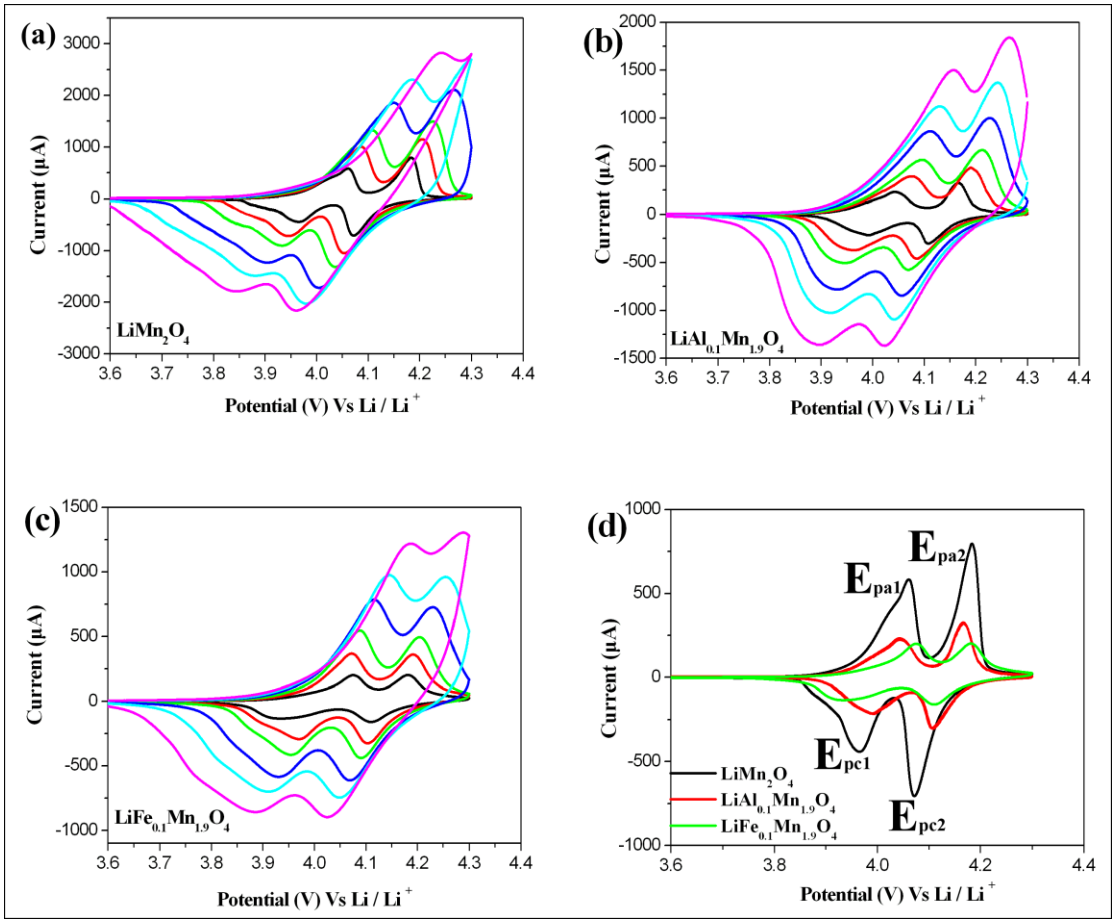

Figure 5. Cyclic voltammograms (CVs) of the electrodes made with (a) $LiMn_2O_4$, (b) $LiAl_{0.1}Mn_{1.9}O_4$ and (c) $LiFe_{0.1}Mn_{1.9}O_4$. In (a)–(c), the scan rates are set at 0.1 (black), 0.2 (red), 0.3 (green), 0.5 (blue), 0.7 (cyan), and 1mV S^{-1}(magenta) from the inside out. (d) Comparison of the CVs recorded at the scan rate of 0.1 mV s^{-1}

Table 3. Summary of the CVs results at the potential scanning rate of 0.1mVs^{-1} and the determined Li^+ diffusion coefficient for the spinel electrodes

electrode	Potential values/mV						Diffusion coefficient/cm^2 s^{-1}	
	E_{pa1}	E_{pa2}	E_{pc1}	E_{pc2}	ΔE_1	ΔE_2	D_{a1}	D_{c2}
$LiMn_2O_4$	4.06	4.18	3.96	4.07	100	110	2.64×10^{-7}	1.46×10^{-7}
$LiAl_{0.1}Mn_{1.9}O_4$	4.04	4.17	3.99	4.11	50	60	8.51×10^{-8}	6.25×10^{-8}
$LiFe_{0.1}Mn_{1.9}O_4$	4.07	4.18	3.94	4.11	140	70	5.54×10^{-8}	2.85×10^{-8}

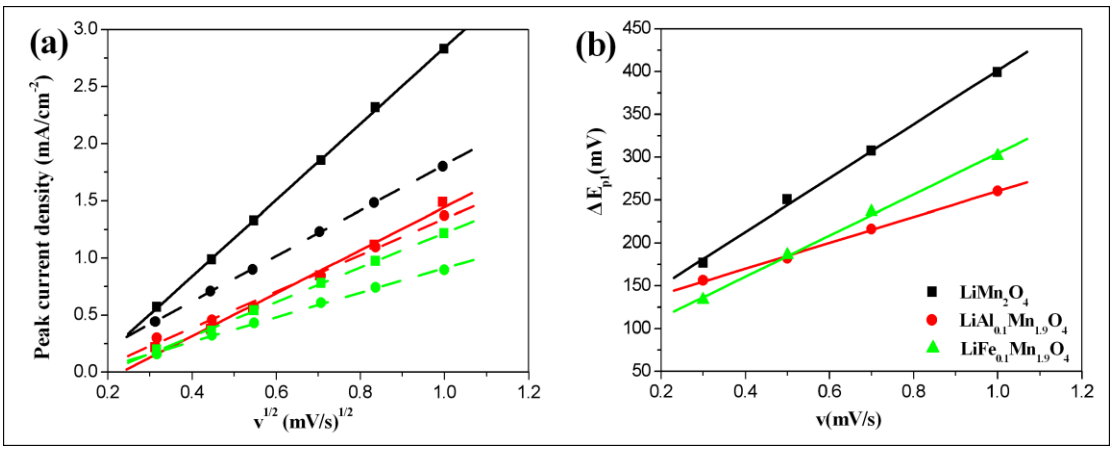

Figure 6. (a) Plots of the peak current density versus the square root of potential scan rate derived from the CVs of $LiMn_2O_4$ (black), $LiAl_{0.1}Mn_{1.9}O_4$ (red) and $LiFe_{0.1}Mn_{1.9}O_4$ (green). Solid lines and dash lines correspond to the E_{pa1} and E_{pc2}, respectively; (b) Widening separation potential within each redox couple (ΔE_{p1}) versus the potential scan rate

The determined data falls within the order of 10^{-8}–10^{-7} cm^2 s^{-1}. It should be noted that the $LiMn_2O_4$ displays relatively larger redox couple separation (ΔE_{p1}) between E_{pa1} and E_{pc1} than those of doped $LiMn_2O_4$ samples as the potential scanning rate (v) increases (Fig. 6b). It is reported that ionic conductivity is not to be dominant in the conductivity of $LiMn_2O_4$ at room temperature [26]. The rate constant for electron transfer is determined from the peak potential separation [27]. The relatively larger redox couple separation displaying by $LiMn_2O_4$ is due to lower rate constant for electron transfer. Fig. 5d compares the CVs of the three spinel electrodes tested at the same rate of 0.1 mV s^{-1}. Seen from Fig. 5d, the cathodic peaks shift to higher potential. This observation coincides with the galvanostatic results showing that the $LiAl_{0.1}Mn_{1.9}O_4$ and $LiFe_{0.1}Mn_{1.9}O_4$ electrodes exhibit higher discharge plateaus. The separation of peak potentials for $LiAl_{0.1}Mn_{1.9}O_4$ are 50 and 60 mV, obviously lower than those of pure $LiMn_2O_4$ sample (100 and 110 mV) and $LiFe_{0.1}Mn_{1.9}O_4$ sample (140 and 70mV) indicating that lithium inserting reaction of $LiAl_{0.1}Mn_{1.9}O_4$ is in a more equilibrium state behaving more likely as a Nernst system. Therefore, $LiAl_{0.1}Mn_{1.9}O_4$ is featured with advantage of better cycle performance compared to $LiMn_2O_4$ and $LiFe_{0.1}Mn_{1.9}O_4$.

3.4 The measurement of EIS

Fig. 7a shows the equivalent circuit for modeling the impedance data. The EIS of the $Li/LiMn_2O_4$, $Li/LiAl_{0.1}Mn_{1.9}O_4$ and $Li/LiFe_{0.1}Mn_{1.9}O_4$ half–cells composed of a semicircle and a straight slopping line are shown in Fig. 7b–7d, respectively. Electrochemical impedance data (points) and the fitted curve (line) calculated with ZSimpWin software measured at the open circuit voltage (OCV) [20]. The R_Ω is bulk resistance of the cell; R_{sei} and C_{sei} are the resistance and the capacitance of the solid-state interface layer formed on the surface of the electrodes; R_{ct} and C_{dl} are the Faradic charge-transfer resistance and its relative double layer capacitance; W is the Warburg impendence (Z_w) related to a combination of the diffusional effects of Li^+. The R_{ct} of $LiMn_2O_4$ (152.4Ω cm^{-2}) is largest

among the three half–cells, while the $LiAl_{0.1}Mn_{1.9}O_4$ displays the lowest R_{ct} (89.3Ω cm^{-2}). This result coincides with the separation of peak potentials with increasing the potential scanning rate. The Z_w values of $LiMn_2O_4$, $LiAl_{0.1}Mn_{1.9}O_4$ and $LiFe_{0.1}Mn_{1.9}O_4$ obtained by fitting the impedance data are 57.4, 65.7, 87.2 Ω cm^{-2}, respectively. This tendency is coincidence with the diffusion coefficient calculated from cyclic voltammetry studies.

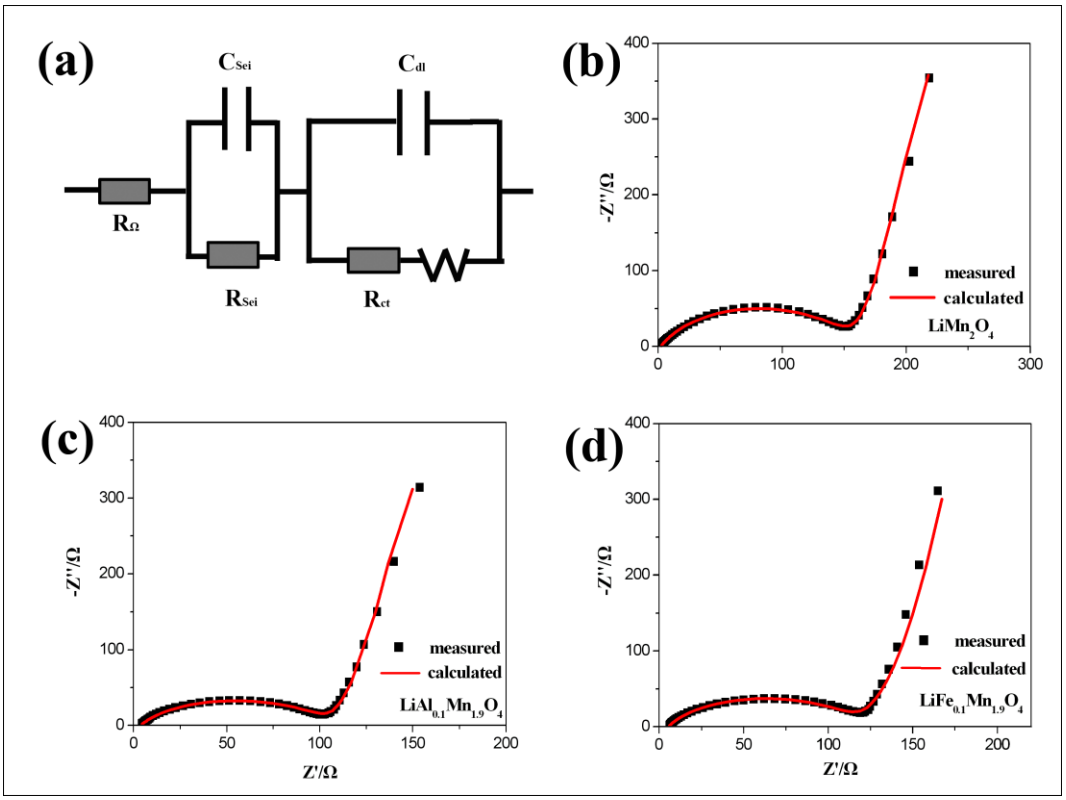

Figure 7. (a) The equivalent circuit for modeling the impedance data. (b–d) Electrochemical impedance data (black points) and the fitted curve (red line) of the samples measured at potential of the open circuit voltage

4. CONCLUSIONS

The spinel $LiM_{0.1}Mn_{1.9}O_4$ (M=Mn, Al, Fe) materials were synthesized using the sol–gel process starting from metal nitrates, citric acid and glycol. TEM shows the grain sizes of the prepared materials are around 100nm. The porous structures formed by aggregation of particles are observed through SEM. The N_2 adsorption/desorption experiments show the relatively big surface area of the samples. The $LiAl_{0.1}Mn_{1.9}O_4$ sample shows the best electrochemical properties both at high rate and at high temperature. A typical $Li/LiAl_{0.1}Mn_{1.9}O_4$ cell shows a discharge capacity of 95.8mAh g^{-1} at 50C discharge rate (5C charge rate) at 25°C. Even at 55°C, capacity retention of 85.0% for 5C rate after 200 cycles is obtained. The lower separation of peak potentials obtained from CVs for $LiAl_{0.1}Mn_{1.9}O_4$ indicates that it is a more equilibrium state compared to $LiMn_2O_4$ and $LiFe_{0.1}Mn_{1.9}O_4$. D_{Li} of the

samples calculated from the CVs data is the order of 10^{-8}–10^{-7} cm^2 s^{-1}. The $LiAl_{0.1}Mn_{1.9}O_4$ exhibits good kinetics properties due to the lowest R_{ct} through the studies of EIS among the three spinel cathodes. The $LiAl_{0.1}Mn_{1.9}O_4$ synthesized in our work is a promising cathode material for applications in both EVs and HEVs.

ACKNOWLEDGEMENTS
This study was supported by the 973 Project of China (No.2011CB935901), the National Natural Science Foundation of China (Grant No. 11179043, No. 91022033) and the Independent Innovation Foundations of Shandong University (2011GN032). We are also grateful to the Graduate Independent Innovation Foundation of Shandong University (yzc11034).

References

1. M. Aklalouch, J. M. Amarilla, R. M. Rojas, I. Saadoune and J. M. Rojo, *Electrochem. Commun.*, 12 (2010) 548
2. H. W. Lee, P. Muralidharan, R. Ruffo, C. M. Mari, Y. Cui and D.K. Kim, *Nano Lett.*, 10 (2010) 3852
3. A. Sakunthala, M. V. Reddy, S. Selvasekarapandian, B. V. R. Chowdari and P. C. Selvin, *Electrochim. Acta*, 55 (2010) 4441
4. K. M. Shaju and P. G. Bruce, *Chem. Mater.*, 20 (2008) 5557
5. Y. L. Ding, J. Xie, G. S. Gao, T. J. Zhu, H. M. Yu and X. B. Zhao, *Adv. Funct. Mater.*, 21 (2011) 348
6. A. B. Yuan, L. Tian, W. M. Xu and Y. Q. Wang. *J Power Sources*, 195 (2010) 5032
7. J. Cho, *J Mater. Chem.*, 18 (2008) 2257
8. L. Wang, J. S. Zhao, S. H. Guo, X. M. He, C. Y. Jiang and C. R. Wan, *Int. J. Electrochem. Sci.*, 5 (2010) 1113
9. H. G öktepe, H. Şahan, and Ş. Patat and A. Ülgen, *Ionics*, 15 (2009) 233
10. F. A. Amaral, N. Bocchi, R. F. Brocenschi, S. R. Biaggio and R. C. Rocha-Filho, *J. Power Sources*, 195 (2010) 3293
11. X. J. Sun, X. H. Hu, Y. Shi, S. X. Li and Y. Q. Zhou, *Solid State Ionics*, 180 (2009) 377
12. W. M. Xu, A. B. Yuan, L. Tian and Y. Q. Wang, *J Appl. Electrochem.* 41 (2011) 453
13. D. Arumugam, G. P. Kalaignan, K. Vediappan and C. W. Lee, *Electrochim. Acta*, 55 (2010) 8439
14. D. Arumugam and G. P. Kalaignan, *J Electroanal. Chem.*, 648 (2010) 54
15. J. M. Amarilla, K. Petrov, F. Picó, G. Avdeev, J. M. Rojo and R. M. Rojas. *J Power Sources*, 191 (2009) 591
16. Y. S. Lee, N. Kumada and M. Yoshio, *J Power Sources*, 96 (2001) 376
17. B. J. Hwang, R. Santhanam, D.G. Liu and Y.W. Tsai, *J Power Sources*, 102 (2001) 326
18. T. F. Yi, Y. R. Zhu, R. S. Zhu, L. Zhou, P. Li and J. Shu, *Ionics*, 15 (2009) 177
19. T. F. Yi, X. G. Hu and K. Gao, *J Power Sources*, 162 (2006) 636
20. S. J. Bao, Y. Y. Liang, W. J. Zhou, B. L. He and H. L. Li, *J Power Sources*, 154 (2006) 239
21. H. J. Bang, V. S. Donepudi and J. Prakash, *Electrochim. Acta*, 48 (2002) 443
22. Q. Luo and A. Manthiram, *J. Electrochem. Soc.*, 156 (2009) A84
23. F. Y. Cheng, H. B. Wang, Z. Q. Zhu, Y. Wang, T. R. Zhang, Z. L. Tao ang J. Chen, *Energy Environ. Sci.*, 4 (2011) 3668
24. L. F. Xiao, Y. Q. Zhao, Y. Y. Yang, Y. L. Cao, X. P. Ai and H. X. Yang, *Electrochim. Acta*, 54 (2008) 545
25. J. A. Dean, *Langes Handbook of Chemistry*, 14th ed, New York (1992)

26. E. Iguchi, Y. Tokuda, H. Nakatsugawa and F. Munakata, *J. Appl. Phys.*, *91* (4) (2002) 2149
27. R. S. Nicholson, *Anal. Chem.*, 37 (1965) 1351